Molecule−Molecule versus Molecule−Substrate Interactions in the Assembly of Oligothiophenes at Surfaces

Mathieu Surin,[†] Philippe Leclère,[†] Steven De Feyter,[‡] Mohamed M. S. Abdel-Mottaleb,[‡] Frans C. De Schryver,[‡] Oliver Henze,[§] W. James Feast,[§] and Roberto Lazzaroni*,[†]

Service de Chimie des Matériaux Nouveaux, Université de Mons-Hainaut, Place du Parc 20, B-7000 Mons, Belgium, Laboratory of Photochemistry and Spectroscopy, Katholieke Universiteit Leuven, Celestijnenlaan 200F, B-3001 Heverlee-Leuven, Belgium, and IRC in Polymer Science and Technology, Durham University, South Road, Durham DH1 3LE, United Kingdom

Received: November 24, 2005

In this paper we present a joint experimental and theoretical approach for the study of the assembly of end-substituted oligothiophenes at surfaces with different polarities (i.e., mica vs graphite). Scanning probe microscopy studies of (sub)monolayer deposits show various types of structures (one-dimensional fibrils, two-dimensional regular layers, and monolayers), depending on the nature of the end groups and the substrate. Using molecular modeling with an atomistic approach, we focus on the interplay between the molecule−molecule (and segment−segment) interactions and the molecule−substrate interactions and their influence on the observed morphologies and the stacking geometry. Such information is relevant for controling the structural order in thin layers of thiophene oligomers for use in field-effect transistor applications, for example, by modifying the nature of dielectric material over which those compounds are deposited.

1. Introduction

Interactions between molecules and a substrate surface are of the utmost importance in thin films/deposits, since they determine the assembly of the molecules in the vicinity of the surface (i.e., in the first monolayer, over which the overlayers then grow). The adsorption process can lead to a significant change of the electronic structure of the adsorbate because of chemical bonding with the substrate (chemisorption); in the case of a relatively weak interaction regime (physisorption), the intrinsic self-assembly of the molecules can be perturbed by specific noncovalent interactions with the substrate surface. In organic semiconductor applications, the interface between the active (semiconducting) polymer/oligomer and the solid surfaces (e.g., electrodes, alignment layer, dielectric surface, etc.) dramatically influences the device performances. For instance, in light-emitting or photovoltaic diodes, the structure of the interface between the electrodes and the active semiconducting layer has been a subject of intensive investigation to improve the diode performances.[1] In the case of organic field-effect transistors (OFETs), the device performances are dramatically influenced by (i) the structural order within the active layer (the packing morphology and the interchain interactions influence the charge transport properties, in particular the charge mobility), (ii) the interface between the dielectric material and the active compound, and (iii) the interface between the electrodes and the active layer.[2] Therefore, understanding of the interplay between the molecular architecture, the structural order arising from intermolecular interactions in the solid state, and the molecule−substrate interactions is needed to improve the device performances.[3] In particular, the study of the assembly within deposits in the submonolayer to few monolayers regime is of paramount importance, since it has been shown that the charge transport in OFETs entirely takes place within the first two monolayers of the active material in the channel, near the dielectric material.[4]

Thiophene-based oligomers and polymers are the prototype conjugated materials in OFETs.[5] Oligothiophene derivatives exhibit various self-assembled structures depending on the interplay between the molecular architecture and the experimental protocol adopted, including the type of substrate over which they are grown, the temperature, the solvent, and concentration, as described by several authors.[6,7] For instance, on apolar substrates such as graphite, passivated silicon (Si−H/Si), and metal surfaces, it has been shown that oligothiophenes (and other conjugated oligomers such as pentacene) orient with their long axis parallel to the surface plane, in some cases in epitaxy with the crystalline lattice of the substrate.[6,8] In contrast, on polar substrates such as mica or oxidized silicon (SiO_x), these molecules are known to orient almost perpendicular to the substrate plane, in their crystalline form.[8,9] Since one can use a variety of dielectric materials (over which the semiconducting layer is deposited) of different polarities (e.g., organic polymers, mica, TiO_2, SiO_x, Si−H, or silanized dielectric substrates), different morphologies can be obtained, which can strongly modify the performances of the OFET devices.[10]

In this context, we present a joint theoretical/experimental study of the assembly of thiophene-based oligomers on two different substrates, i.e., muscovite mica and graphite, with strongly contrasting polarities; muscovite mica is an aluminosilicate ionic mineral (strongly polar/hydrophilic) while graphite is an apolar, hydrophobic substrate.[11] Muscovite mica and graphite surfaces are particularly well suited for this study, since they are easily cleavable, chemically clean, and atomically flat.

* Author to whom correspondence should be addressed. E-mail: Roberto@averell.umh.ac.be.
[†] Université de Mons-Hainaut.
[‡] Katholieke Universiteit Leuven.
[§] Durham University.

10.1021/jp056824q CCC: $30.25
Published on Web 03/30/2006

SCHEME 1: Chemical Structures of the Studied Compounds

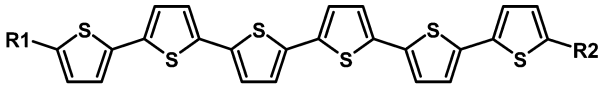

T_6 : R1=R2= H

$(EO)_5$-T_6-Hex : R1= *n*-C6H13 ; R2=

$(EO)_5$-T_6-$(EO)_5$: R1=R2=

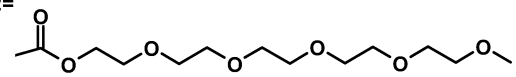

This allows us to analyze ultrathin deposits (in the submonolayer/few layers regime) with atomic force microscopy (AFM). This technique provides surface topographic imaging with a lateral resolution of a few nanometers and a vertical resolution around 1 Å. The morphological information obtained with AFM can then be compared to scanning tunneling microscopy (STM) data collected at the liquid/graphite interface with angstrom lateral resolution to better understand the molecular packing inside monolayers. Here, we report on the adsorption/assembly processes of oligothiophene derivatives on those substrates; we consider sexithiophene-based molecules, substituted on the α,*ω*-positions by two oligo(ethylene oxide) groups ("symmetric molecule", $(EO)_5-T_6-(EO)_5$) or by one alkyl group in α and one oligo(ethylene oxide) group in *ω* ("asymmetric molecule", $(EO)_5-T_6-$Hex); see Scheme 1. (Their synthesis is described in ref 12.) In contrast to the unsubstituted oligothiophene (T_6, see Scheme 1), the studied compounds are soluble in common organic solvents, allowing us to generate deposits from solution. The results of AFM/STM morphological studies are compared to molecular modeling by means of molecular mechanics (MM) and molecular dynamics (MD) simulations. In the first step, we model the interactions between a single molecule and the substrate to understand the interactions of each segment with the surface. In the second step, we simulate stacks of molecules onto substrates and compare the results with morphological studies. Finally, we rationalize the results of molecular modeling in terms of molecule−molecule versus molecule−surface interactions.

2. Methodology

2.1. Scanning Probe Microscopy. For AFM investigations, thin deposits were prepared by solvent-casting (to avoid aggregation in solution, we used solvents in which the solubility of the compounds is high, such as tetrahydrofuran (THF) or toluene) on freshly cleaved muscovite mica and highly oriented pyrolytic graphite (HOPG) from dilute solutions (0.1 mg/mL). The solvent was slowly evaporated at room temperature in a solvent-saturated atmosphere. Tapping-mode atomic force microscopy was performed with a Nanoscope IIIa microscope from Veeco (operating in air, at room temperature). The instrument is equipped with the Extender Electronics Module to provide simultaneously height and phase cartography. Microfabricated silicon cantilevers were used with a spring constant of ∼30 N m^{-1}. Images of different areas of the samples were collected with the maximum available number of pixels (512) in each direction. The Nanoscope III, version 5.12, image processing software was used for image analysis.

In the STM investigations, performed at Katholieke Universiteit Leuven, a droplet of a solution of $(EO)_5-T_6-$Hex in phenyloctane (0.5 mg/mL) was cast on a freshly cleaved HOPG surface. The STM images were acquired in the variable-current mode (constant height) under ambient conditions. In the STM images, bright areas correspond to the highest and dark areas to the lowest measured tunneling current. STM experiments were performed using a Discoverer scanning tunneling microscope (Topometrix, Inc., Santa Barbara, CA) along with an external pulse/function generator (model HP 8111 A), with negative sample bias. Tips were electrochemically etched from a Pt/Ir wire (80%/20%, diameter 0.2 mm) in a 2 N KOH/6 N NaCN solution in water. After a STM image of a monolayer structure was recorded, the underlying graphite surface was imaged at the same position for calibration, by decreasing the bias voltage.

2.2. Molecular Mechanics and Molecular Dynamics Simulations. All MM and MD simulations were performed using the Universal Force Field (UFF 1.02)[13] available in Cerius2 and Materials Studio 3.0 packages by Accelrys, since it accurately reproduces the geometry of oligothiophenes in their crystalline structure as well as the geometry and the torsional behavior of saturated chains such as hydrocarbons and oligoethers. UFF has also been designed to simulate main-group inorganic compounds and provides an accurate description of interactions between clay minerals and organic molecules.[14]

2.2.1. Single Molecules. For 2,2′-bithiophene, the UFF force field gives the most stable structure where the thiophene units are antiplanar (S−C−C−S torsion angle of 180°), which is adequate to simulate the *solid-state* behavior of conjugated compounds. (Oligothiophenes are indeed planar in the solid state.) Atomic charges are assigned using the PCFF force field, which correctly ascribes the atomic charges of organic molecules, which are then imported in the UFF calculation. Conformer search by grid scan MM was applied to find the most stable conformers of the molecules. For the energy minimization, the conjugate gradient (Polak−Ribiere) algorithm was used with root-mean-square (RMS) force convergence criterion set at 10^{-3} kcal mol^{-1} $Å^{-1}$. For simulating molecular stacks, UFF also appears to be the best force field, since it properly describes the low-temperature crystalline structure of T_6 upon applying a MM procedure on the periodic lattice.

2.2.2. Construction of Substrate Surfaces. Muscovite mica is a $2M_1$ alumino-silicate-based layered mineral, with a general unit cell formula of $KAl_2(Al,Si_3)O_{10}(OH)_2$. The structure was built from the crystal structure given in Cerius2. Although the real muscovite mica structure corresponds to a blend of interlayer cations (depending on its origin, K^+, Na^+, Ca^{2+}, and Ba^{2+} cations can be found in various proportions), we have considered for the sake of simplicity a structure in which the interlayer is only filled with K^+ ions, since they always represent between 88% and 99% of the molar fraction of interlayer cations.[15] The structure was cleaved along its *c* direction to obtain a single layer, and a superlattice was created to obtain *a* × 8; *b* × 6 (41.55 Å × 53.976 Å) or *a* × 4; *b* × 3 (20.776 Å × 26.988 Å) periodic lattices, with a *c* axis being a vacuum slab of few tens of angstroms (depending on the studied system,

from 30 to 80 Å). Atom charges were assigned following the description given in comparable clay mineral systems[16] (Appendix). Half of the K^+ ions were randomly removed from the surface for preserving the electrical neutrality of the crystal after cleaving along *c*; this reflects the surface structure of muscovite mica after cleaving for the purpose of elaborating deposits.[17] The layer atoms were kept fixed in their position, while K^+ ions were allowed to move in a MM procedure to relax the crystal surface. This leads to a slight movement of these ions toward the silicate cavities of the layer; the distance between K^+ ions and the basal plane evolves from 1.6 to 1.4−1.5 Å, in full agreement with simulations described in ref 18. On the basis of that structure, a MD run was carried out, in which the K^+ ions surface (48 atoms) were free to move. The self-diffusion constant, calculated from the mean-square displacement of all K^+ ions, is $D = 0.1319 \times 10^{-3}$ A^2 ps^{-1} atom^{-1}. This very low value allows us to consider that these ions can be fixed in their position prior to any MD simulation of molecule−substrate interactions. This also allows us to focus on the dynamics of the molecule itself and to compare energy values between different systems, and it reduces the computational effort.

The model graphite substrate has been built as two graphitic layers, each of 20 × 20 six-membered fused rings in a periodic lattice, with a *c* axis being a vacuum slab of 50 Å.[19]

2.2.3. Simulations of Molecule−Substrate Interactions. The molecule was initially placed with the conjugated plane parallel to the surface of the substrate, typically 8 Å from the surface plane. Note that all simulations were carried out with periodic boundary conditions to avoid edge effects. The atoms of the substrate were kept fixed in their position, since physisorption is not expected to alter the geometry of the substrate surface. A first MM procedure was applied with no charge equilibration. MD simulations were then performed using the canonical ensemble (constant *N*, *V*, *T*) with the Nosé−Hoover thermostat. Simulations were carried out using the so-called "Verlet-leapfrog" algorithm with a relaxation time of 0.1 and a time step of 1 fs. The temperature of the system was gradually increased from 10 K up to 300 K by steps of 10 K during 5 ps; this allows a gradual increase in kinetic energy of the system that globally leads to a system in equilibrium when the temperature reaches 300 K. At this temperature, the simulation keeps running during 300 ps with a time step of 1 fs (one output frame is generated every 50 fs). This time scale allows the movement of a single molecule over the whole surface plane of the periodic lattice, therefore probing all the possible sites of interaction. The stable structures refer to the potential energy minima over the whole trajectory file. A MM procedure was finally applied to the first few minima to identify the most stable structures. For all the simulation steps (MM and MD), the nonbonded van der Waals interactions were described using the Spline method (with cut-on and cut-off parameters set to 9.0 and 12.0 Å, respectively), while electrostatic interactions were described using the Ewald summation method for periodic systems.

The building of stacks of a few molecules was carried out following the experimental evidence about the morphology (see below). Note that the number of molecules considered in the layer over mica with a periodic lattice $a \times 4$; $b \times 3$ was calculated from a mean density between those of PEO and T_6 (1.13 and 1.55 g/cm^3, respectively) and taking into account the experimental data of the measured thicknesses of the monolayers (see below). The same methodology (MM + MD) was applied for simulating the interactions between those stacks of molecules and the substrate.

3. Results

The results are presented in four sections; the first section reports the experimental results obtained by scanning probe microscopy techniques of (sub)monolayer deposits. Next, we model the interaction of a single molecule on graphite and mica to identify the specific interactions between the different segments of the molecules and these surfaces. The third section briefly describes the in-stack intermolecular interactions for two types of stacking configurations: the crystalline herringbone structure and the face-to-face π-stacking structure, which both have been observed experimentally for thiophene-based oligomers. Finally, the last section is devoted to the modeling of stacks of a few molecules at the substrate surface, in correlation with the experimental results.

3.1. Microscopic Morphology of Thin Deposits. We have recently reported on the AFM investigations of the microscopic morphology of thin deposits of a series of α,ω-substituted oligothiophenes.[6] Here we only consider the structures that result from self-assembly on the surfaces (rather than preaggregation in solution), via deposition either from the vapor phase (for unsubstituted T_6) or from good solvents (for the substituted derivatives). Vacuum-sublimed deposits of T_6 on polar substrates (mica, SiO_2)[20] show a layered-type morphology; the thickness of the terraces is constant, approaching the length of a molecule along its long axis (23.9 Å), while the lateral extension of the layers can vary widely, up to a few micrometers. These structures result from the crystallization process when the oligomers arrange in a herringbone motif laterally (in the plane of the substrate) as observed by X-ray diffraction,[21,22] while vertically (along the *c* direction of the crystal, perpendicular to the substrate plane) the molecules are only slightly interacting, producing therefore a layered morphology. However, for deposits on apolar substrates such as graphite or Si−H, the molecules tend to orient with their long axis parallel to the substrate, suggesting stronger molecule−substrate interactions.[7a]

For thin deposits of $(EO)_5-T_6-Hex$ on mica, a similar situation is obtained: multilayered islands form, as shown in Figure 1a. In this AFM image, the mica substrate appears dark, while each layer appears in a different gray contrast (bright areas corresponding to higher parts of the image); the lateral extension of successive overlayers tends to decrease, producing stepped pyramid-like objects (as the object in the left part of the image, in which 10 layers are stacked). The thickness of all the layers is constant, i.e., 4.7 ± 0.2 nm. This is close to the length of the fully extended molecule (5.10 nm), suggesting that the molecules are in the same type of packing as T_6 on polar substrates. This is also reminiscent of the description by Garnier et al.[22] of the self-assembly in layers of $Hex-T_6-Hex$, in which the molecules are almost perpendicular to the layer plane for deposits on polar substrates.

For thin deposits of $(EO)_5-T_6-(EO)_5$ on mica, a layered morphology is also observed, as shown in Figure 1b (substrate in dark, layers in gray). Again, the thickness of the layers is constant, i.e., 2.7 ± 0.2 nm. However, thin deposits of $(EO)_5-T_6-(EO)_5$ on mica differ from those of $(EO)_5-T_6-Hex$ by two aspects: (i) The value of the layer thickness for $(EO)_5-T_6-(EO)_5$ is small compared to the length of the fully extended molecule (6.57 nm). Therefore the molecules are not fully extended perpendicular to the mica plane, in contrast to the case of $(EO)_5-T_6-Hex$. (ii) In the case of $(EO)_5-T_6-(EO)_5$, no stacked layers appear before quasi-full coverage of the substrate by the first monolayer, in contrast to the previous case where a lot of stacked layers appears even when the substrate is not fully covered. The latter issue is reminiscent of the differences in

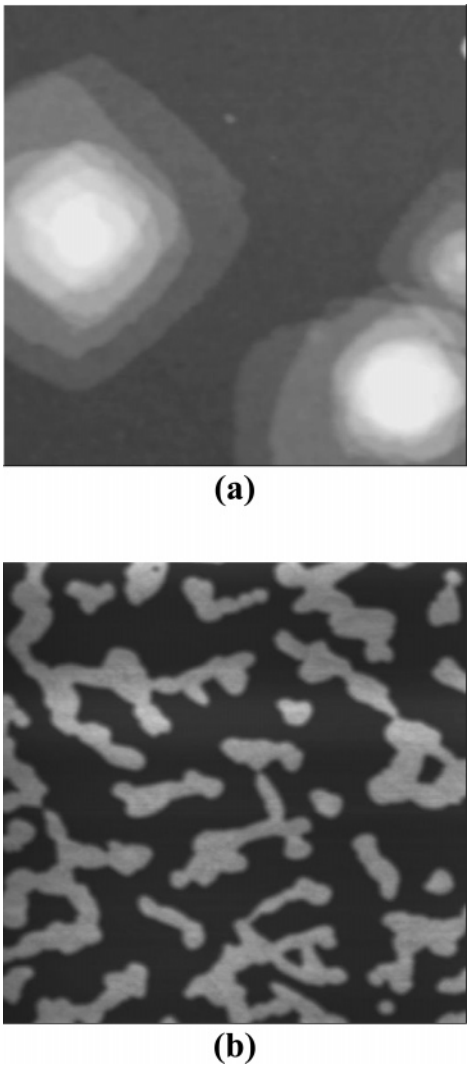

Figure 1. AFM images ($1.5 \times 1.5\ \mu m^2$) of thin deposits on mica of (a) $(EO)_5-T_6-Hex$ and (b) $(EO)_5-T_6-(EO)_5$. The vertical gray scale is 75 and 7 nm for parts a and b, respectively.

the microscopic morphology for different growth modes; the case of $(EO)_5-T_6-Hex$ resembles the case of the "island" mode (Volmer−Weber) while the case of $(EO)_5-T_6-(EO)_5$ is reminiscent of the "layer-by-layer" mode (van der Merwe). The morphological difference between these growth modes stems from differences in terms of adsorbate−substrate interactions, which are larger than adsorbate−absorbate interactions in the layer-by-layer case while it is the opposite for the island mode.[23] Note that these models were initially developed for describing deposits from the vapor phase; in our case, since the different morphologies appear for deposits from the same (good) solvent, we believe that those morphologies arise from the interplay between molecule−molecule and molecule−substrate interactions, which are the interactions taken into account in those models of growth, with little influence of the solvent.

For thin deposits on graphite, the differences in terms of microscopic morphology between $(EO)_5-T_6-(EO)_5$ and $(EO)_5-T_6-Hex$ are even more pronounced. For $(EO)_5-T_6-(EO)_5$, the deposits do not show any type of layered morphology; instead, well-defined one-dimensional (1D) objects are observed; see Figure 2a. These objects (in gray) have a constant thickness of about 1 nm and widths of a few nanometers to tens of nanometers, while the length varies from tens of nanometers to several micrometers. Careful measurements on these objects lead to the conclusion that their width is an integer multiple of about 6−7 nm, i.e., about the length of the fully extended molecule (6.57 nm). This was confirmed by STM studies,[24] which showed that these objects are made of side-by-side stripes, each a single molecule wide. This suggests that π-stacking occurs along the long axis of these objects, with the molecules perpendicular to the stacking direction. Note that these objects are oriented according to a 3-fold symmetry, reminiscent of that of the crystalline lattice of graphite, which suggests a particular interaction of the molecules with this substrate.

The microscopic morphology of thin deposits of $(EO)_5-T_6-Hex$ on graphite is shown in Figure 2b. In this image, we observe the presence of three levels of topographic contrast. The small dark regions correspond to the graphite substrate ("lowest" areas). The gray area corresponds to a monolayer 3 ± 1 Å thick, suggesting an arrangement in which the long axis of the molecules is likely to be parallel with respect to the graphite surface. On top of this monolayer we observe thicker layers (bright), with a thickness around 4.7 ± 0.2 nm. The latter value is similar to the layers on mica, with the molecules almost perpendicular to the substrate plane. To determine the packing inside the first monolayer of 3 ± 1 Å (the one directly interacting with graphite), we use STM, which is a powerful tool to investigate such types of monolayers, in particular at the solution−graphite interface.[25] Using a dilute solution of $(EO)_5-T_6-Hex$ in 1-phenyloctane (i.e., a good solvent, chosen for its very low evaporation rate), monolayers spontaneously form after a while, and STM current images were recorded (Figures 2c and 2d). In these STM images, bright regions correspond to a higher tunneling current than dark regions, which is usually associated with π-conjugated systems due to the lower energy gap between their frontier electronic levels and those of graphite, compared with saturated alkyl or alkoxy chains.[26] In Figure 2c, we observe small bright spots that are packed very regularly in small domains separated by straight boundaries. From the STM image in Figure 2d, the elongated objects are undoubtedly conjugated segments, since their dimensions equal those of T_6 segments. The molecules are ordered in a two-dimensional (2D) lattice with the following unit cell parameters (yellow): $a \times b = 22 \times 31$ Å^2; $\alpha = 120°$. The latter value suggests a quasi-epitaxial growth of the monolayer, since it follows the 3-fold symmetry of the graphite surface. The fact that the packing is loose (the molecules do not seem to be in close contact with each other) cannot be easily rationalized and will be discussed in more detail in the modeling section. Note that this type of ordering, where the oligothiophene plane is parallel to the substrate, has been described by several authors for other oligothiophene derivatives and is most probably due to the strong interaction between the conjugated segment and the graphite surface.[7,21] For example, Rabe et al.[27] have shown that $Hex-T_6-Hex$ molecules are adsorbed on graphite with their conjugated plane parallel to the substrate in 2D crystals and the packing is dense (one molecule per unit cell of 3.16 nm^2), while in case of $(EO)_5-T_6-Hex$ studied here the size of the unit cell is 6.82 nm^2. This difference in the unit cell size cannot simply be related to the fact that the $(EO)_5-T_6-Hex$ molecule has a larger van der Waals volume than $Hex-T_6-Hex$. To gain further insight on this issue and more globally on the interplay between molecule−substrate and molecule−molecule interactions, the results of the molecular modeling simulations are presented and interpreted in the next three sections.

3.2. Interactions between a Single Molecule and the Substrate. In this section we particularly focus on the stable adsorption geometries that arise from specific interactions between the different segments of the molecules and the

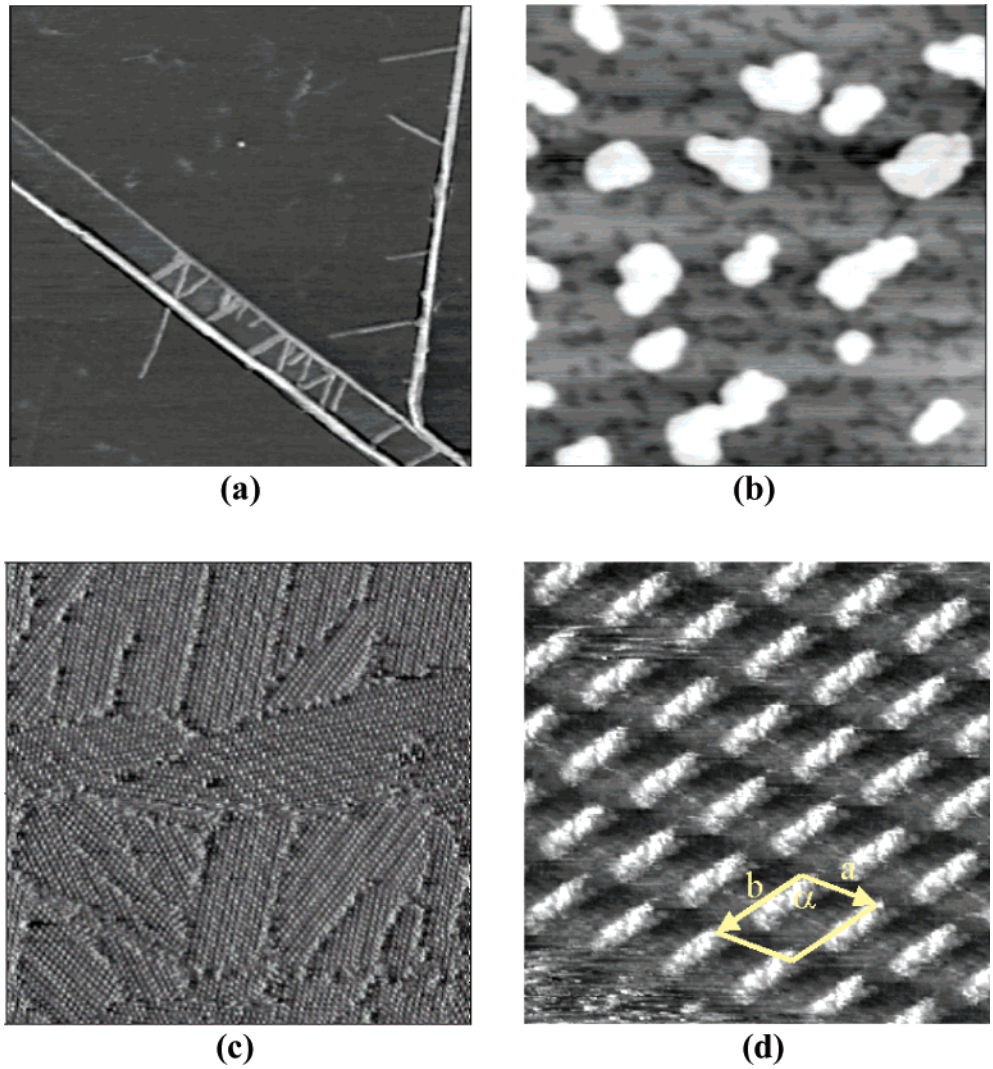

Figure 2. Top: 1.5 × 1.5 μm^2 AFM images of thin deposits on graphite of (a) $(EO)_5-T_6-(EO)_5$ and (b) $(EO)_5-T_6-$Hex. Bottom: STM current images of $(EO)_5-T_6-$Hex at the liquid/graphite interface: (c) 170 × 170 nm^2, $I_t = 0.4$ nA, $V_t = -0.82$ V; (d) 14 × 14 nm^2, $I_t = 1.2$ nA, $V_t = -0.50$ V.

substrate surface as well as on the dynamics and the energetics of the adsorption process.

The most stable structures that have been extracted from the MD run are further refined with a MM optimization; one of these structures is shown in Figure 3 for $(EO)_5-T_6-$Hex. On mica (left), the oligo(ethylene oxide) group interacts with the randomly distributed potassium ions through the interactions between K^+ and O lone pairs; five oxygen atoms (red) of this group complex four potassium ions (mauve) in total. This is also found for all of the stable structures of $(EO)_5-T_6-(EO)_5$ on mica, which clearly indicates that the EO segment strongly interacts with mica via the complexation of the K^+ ions. The equilibrium complexation distance between potassium and oxygen (taken from the radial distribution function (RDF)[28] over the whole MD run) is 2.75 Å, which is identical to the O−K distance in the (18-crown ether-6)$-K^+$ complex.[29] The T_6 segment is adsorbed with the conjugated plane nearly perpendicular to the mica layer plane and slightly distorted from planarity. The T_6 segment cannot adsorb flat on the surface due to its too large van der Waals volume compared to the compactness of the K^+ layer. This orientation of the T_6 segment is similar to that of the T_6 monolayers deposited on mica from the vapor phase.[20] No specific orientation of the alkyl segment with respect to the mica layer is observed.

The stable structures on graphite, as shown in Figure 3b for the case of $(EO)_5-T_6-$Hex, strongly differ from those on mica. On graphite, the molecules tend to accommodate with the conjugated plane lying parallel to the substrate at an equilibrium distance of 3.5−3.6 Å. This distance is typical for $\pi-\pi$ stacking systems[30] (in this case T_6 and graphite). Moreover, for the most stable structures, the hexyl and $(EO)_5$ segments are fully extended, oriented epitaxially with respect to the graphite symmetry; their hydrogen atoms are located above the centers of six-membered rings of the nearest graphitic plane (blue). This geometry has been observed experimentally in the epitaxial ordering of alkanes on graphite;[31] these interactions are therefore very likely to contribute significantly to the epitaxial growth of $(EO)_5-T_6-$Hex on graphite observed in the STM results presented above.

To understand the different energetic contributions to the adsorption, we then performed adsorption energy curves by determining the relative energy versus the molecule−substrate vertical distance for the stable configuration extracted from simulations of $(EO)_5-T_6-$Hex on both substrates. The contributions from the different segments to the total adsorption energy are plotted in Figure 4. These curves can be considered as potential energy curves (the zero energy corresponds to "infinite" separation); the depth of the well reflects the strength of the

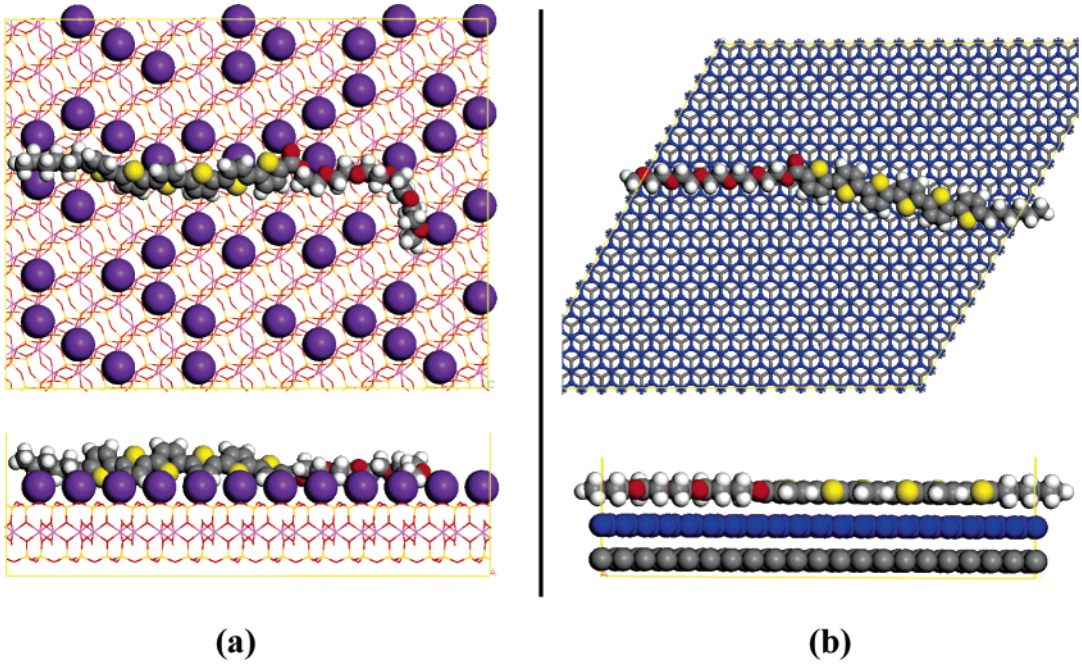

Figure 3. Stable structures for single $(EO)_5-T_6-Hex$ molecules adsorbed on mica (left, the $(EO)_5$ group is on the right side of the molecule) and on graphite (right, the $(EO)_5$ group is on the left side of the molecule), shown with the substrate plane parallel (top) and perpendicular (bottom) to the view.

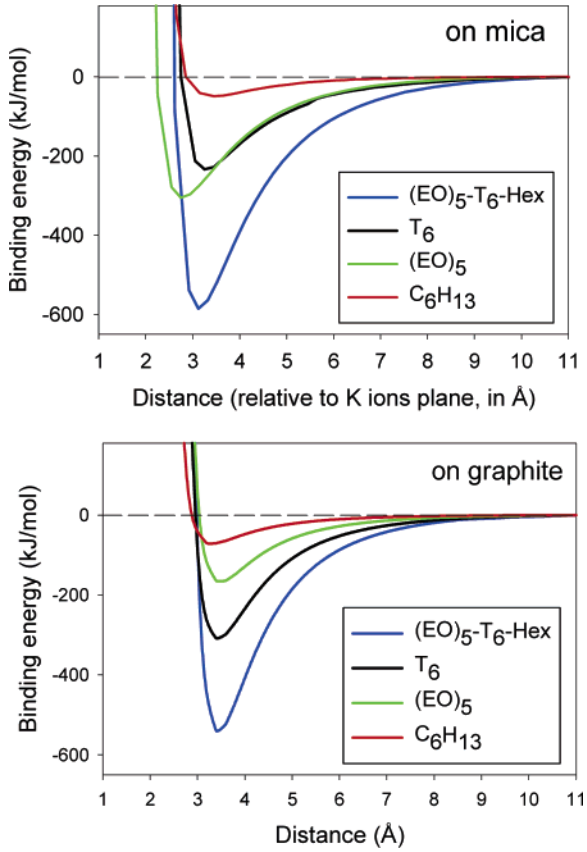

Figure 4. Binding energy of $(EO)_5-T_6-Hex$ adsorbed on mica (top) and graphite (bottom) vs the distance to the substrate plane.

interaction, and the location of its minimum determines the equilibrium distance between the molecule (or the segment) and the substrate. On mica, it is clear that the $(EO)_5$ group is more strongly interacting with the surface (complexation K^+-O lone pairs) compared to T_6, although T_6 and $(EO)_5$ have the same number of atoms, i.e., 42. The hexyl segment (19 atoms) has a very small interaction with this surface. Moreover, the equilibrium distance is different for the different segments; the $(EO)_5$ segment tends to be near the basal K^+ plane (2.7−2.8 Å), while the other two segments are located at an equilibrium distance larger than 3.3 Å. This highlights the fact that the polar segment strongly interacts with the polar mica surface, while the nonpolar segments have a relatively small interaction. In contrast, on graphite the T_6 segment interacts more strongly with the surface ($\pi-\pi$ interactions), while the $(EO)_5$ group has a relatively small interaction compared to that on mica. The hexyl segment is interacting more favorably with graphite (the potential well depth is 71.1 kJ/mol) than with mica (the potential well depth is 49.0 kJ/mol). Note that the value of the well depth for the hexyl group on graphite is very close to the experimental value of the desorption energy for hexane on graphite (74.0 kJ/mol),[32] which is a clear indication of the reliability of the modeling.

The total adsorption energies and their different contributions (internal and nonbonded van der Waals and electrostatic energies) for the stable structures of the different molecules on graphite and mica are listed in Table 1. Note that the adsorption energy is defined as

$$\Delta E_{ads} = E_{tot} - E_{subst} - E_{molec}$$

where E_{tot} is the energy of the whole system, E_{subst} is the total energy of the substrate (both calculated using periodic boundary conditions), and E_{molec} is the total energy of the isolated molecule in its most stable configuration. The adsorption energy includes different contributions, namely, the internal adsorption energy (that is the sum of all the bonded terms, i.e., corresponding to the molecular geometry) and nonbonded terms, van der Waals and electrostatic adsorption energies

$$\Delta E_{ads} = \Delta E_{intern} + \Delta E_{vdW} + \Delta E_{ES}$$

The values calculated for those contributions (listed in Table 1) cannot be directly compared with experimental measurements, which give a single global value for the adsorption energy. Nevertheless, useful comparisons can be made within a given

TABLE 1: Adsorption Energies of the Molecules on Mica and Graphite, in kJ/mol (ΔE_{ads}), with the Contributions from Electrostatic (ΔE_{ES}), van der Waals (ΔE_{vdW}), and Internal (ΔE_{intern}) Energies

	on mica				on graphite			
molecule	ΔE_{ads}	ΔE_{ES}	ΔE_{vdW}	ΔE_{intern}	ΔE_{ads}	ΔE_{ES}	ΔE_{vdW}	ΔE_{intern}
T_6	−245.6	−89.1	−162.8	+6.3	−322.2	−0.8	−322.6	+1.2
$(EO)_5-T_6-Hex$	−521.3	−264.4	−329.3	+72.4	−589.1	−3.8	−592.4	+7.1
$(EO)_5-T_6-(EO)_5$	−661.5	−381.2	−380.7	+100.4	−593.7	+77.0	−703.7	+33.0

row or a given column. The more negative the value, the stronger the interaction between the molecule and the substrate.

The first observation is that for T_6 and $(EO)_5-T_6-Hex$ the adsorption energies are larger (in absolute value) on graphite than on mica (i.e., these molecules are more strongly "bonded" to graphite than to mica). The opposite situation is found for $(EO)_5-T_6-(EO)_5$, due to very strong electrostatic interactions (ΔE_{ES}), which are as large as the van der Waals interaction for this compound on mica. For a given molecule (single row), the difference in energy between mica and graphite is that the interaction with graphite is purely van der Waals, while on mica the total adsorption has significant contributions from both electrostatic (K^+-O lone pairs interactions) and van der Waals terms. These results also indicate that on mica the two substituted molecules are significantly distorted from their most stable configuration (ΔE_{intern} is positive), probably as a consequence of the conformational changes induced in the $(EO)_5$ group(s) upon complexation with the K^+ ions. In contrast, the molecules do not undergo significant geometric changes upon adsorption on graphite compared to their initial geometry.

3.3. Molecule−Molecule Interactions. Here we consider two types of packing, which correspond to observed (crystalline) structures for conjugated oligomers: "π-stack" (face-to-face) and "herringbone" (T-shape) structures.[33] In the former, the conjugated planes are in front of each other; i.e., the 1D stacking direction is perpendicular to the conjugated planes. In the herringbone structure, adjacent chains are in a quasi-T-shape stacking geometry; i.e., a 2D packing is formed. For the simulations of the molecule−molecule interactions, those two types of structures were considered. In our modeling approach, these packing geometries correspond to potential energy minima. In Figure 5 (left), the low-temperature herringbone crystalline polymorph of T_6 is shown. The unit cell (space group $P2_1/n$) has the following structural parameters: $a = 44.71$ Å; $b = 7.85$ Å; $c = 6.03$ Å; $b = 90.8°$ (density = 1.55 g/cm^3).[34] Those crystals present a morphology of layered-type 2D structures, with the long chain axis oriented almost perpendicular to the substrate plane. In the π-stack structure (Figure 5, right), the conjugated planes are parallel, in front of each other, at an equilibrium distance of 3.6 Å. Adjacent chains are displaced relative to each other by nearly half a thiophene unit (1.6 Å) along the molecular axis; this geometry corresponds to a balance between van der Waals interactions (that tend to lead to a fully cofacial stacking geometry) and electrostatic interactions (that tend to repel equivalent atoms in adjacent molecules, as they have identical electrical charges).

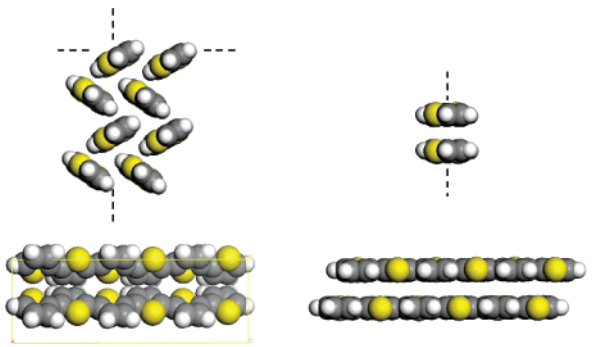

Figure 5. Herringbone (left) and π-stacking (or cofacial, right) types of packing for T_6. Top: View from the short molecular axis. Bottom: View from the long molecular axis (yellow lines represent the crystalline unit cell).

We have considered these two geometries in 1D (π-stack) and 2D (herringbone) periodic lattices for T_6, which both correspond to energy minima. Hereafter we define the *binding energy per molecule* for molecule−molecule interactions as $E_{b,M-M} = (E_{tot} - nE_{molec})/n$, E_{tot} being the total energy of the periodic cell, E_{molec} the energy of an isolated molecule in its most stable configuration, and n the number of molecules. We find binding energy values amounting to −290.4 and −133.9 kJ/mol for the herringbone and π-stack structures, respectively. The fact that the former is larger in absolute value (i.e., more stable) stems from the fact that molecules are surrounded by other ones in two dimensions for the herringbone crystal, while in the cofacial configuration the molecules interact only in one dimension. Interestingly, we note that the binding energy per molecule in the herringbone structure (−290.4 kJ/mol) lies between the total adsorption energy for an isolated molecule on mica (−245.6 kJ/mol, short axis of the conjugated plane perpendicular to the substrate) and graphite (−322.2 kJ/mol, conjugated plane parallel to the substrate). Therefore, it is more stable for a single T_6 molecule to be adsorbed and lie flat on graphite than to be in a herringbone-type of assembly (stabilization by 31.8 kJ/mol), while on mica it is less stable than in the molecular assembly (destabilization by 44.8 kJ/mol). From the energetic point of view, this explains why in T_6 (sub)monolayer deposits, the molecules orient with their long axis parallel to graphite (so neither π-stack structures nor herringbone-type structuresare formed) while on mica they are found perpendicular, most probably in the herringbone-type assembly (using the same preparation conditions).[7a]

For the substituted compounds, we have applied MM in periodic cells of herringbone and π-stacking configurations. Both structures appear stable (local minima) for $(EO)_5-T_6-(EO)_5$ and $(EO)_5-T_6-Hex$. In the case of $(EO)_5-T_6-Hex$, the most stable configurations are, as expected, found when similar saturated segments interact on the same side of the stack (i.e., Hex−Hex on one side and $(EO)_5-(EO)_5$ on the other side, for both types of assemblies). The energy differences in $E_{b,M-M}$ between the herringbone and the π-stack assemblies are −172.4 and −275.7 kJ/mol for $(EO)_5-T_6-(EO)_5$ and $(EO)_5-T_6-Hex$, respectively, in favor of the herringbone assembly. This indicates that, even though the herringbone assembly is more stable than the π-stack assembly in both cases, it is less difficult (in terms of energy) to form a π-stack assembly for $(EO)_5-T_6-(EO)_5$ than for $(EO)_5-T_6-Hex$, when, for instance, sufficient interactions with a substrate promote this type of assembly (see below). This is consistent with the description of Curtis et al.[33] showing that the addition of polar groups (such as PEO) in the α,ω-positions of conjugated oligomers can promote π-stacking.

3.4. Stacks of Molecules Interacting with the Substrate. We particularly focus on the modeling of the observed mor-

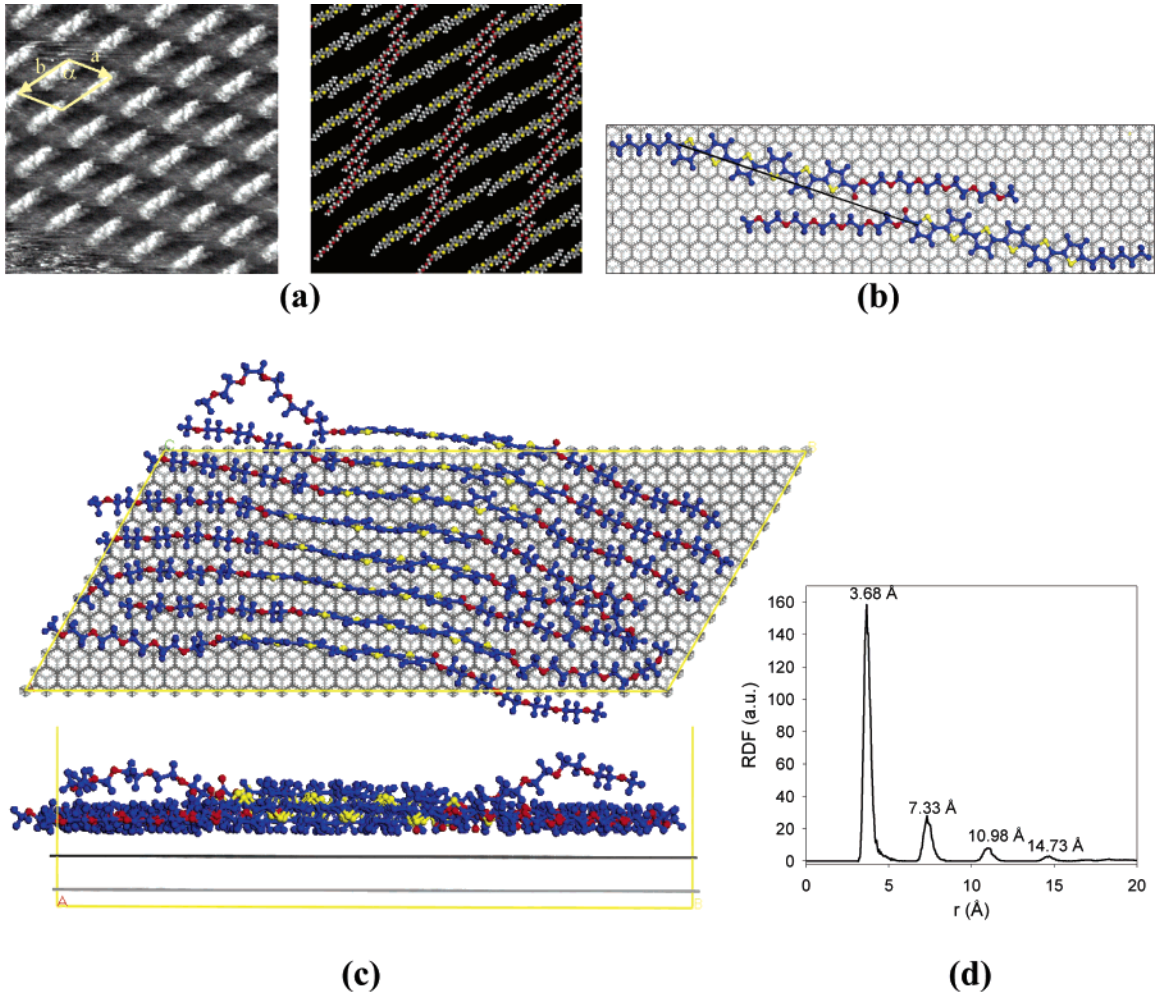

Figure 6. (a) STM image (14 × 14 nm^2) of a monolayer of (EO)$_5$−T$_6$−Hex physisorbed at the 1-phenyloctane−graphite interface (left) and the respective molecular model (right). (b) Molecular modeling of a cluster of two (EO)$_5$−T$_6$−Hex molecules on graphite. (c) Molecular modeling of a cluster of eight molecules of (EO)$_5$−T$_6$−(EO)$_5$ (a × 13; b × 30 cell, with periodic boundaries in yellow). (d) Radial distribution function over the whole MD simulation between equivalent carbon atoms of the T$_6$ segments for the (EO)$_5$−T$_6$−(EO)$_5$ stack on graphite.

phologies in terms of intermolecular structural order and the resulting interactions with the substrate. Comparison between structures on mica and graphite highlights the balance between molecule−molecule and molecule−substrate interactions, which are described in an energetic map.

3.4.1. Structural Order in Stacks on Graphite. For (EO)$_5$−T$_6$−Hex on graphite, STM reveals a loose packing (unit cell/molecule = 6.82 nm^2), suggesting that the intermolecular interactions are very weak while the molecule−substrate interactions are maximized since the conjugated planes are parallel to the graphite plane. In Figure 6a, a molecular model (center) of the STM image (left) is shown, considering that the bright objects are the conjugated segments (section 3.1) and that similar saturated segments ((EO)$_5$ or hexyl) interact more favorably between themselves than with different segments. In this model, the molecules interact only via the saturated groups. This configuration, simulated with a two-molecule cluster on graphite, is shown in Figure 6b, taking into account the distance between molecules from the STM data (black line) and the model for single molecule−graphite interactions (Figure 3b). The hexyl chain and part of the (EO)$_5$ segments are commensurate to the graphite lattice. The shortest distance the between hydrogen atoms on one (EO)$_5$ group and the oxygen atoms of (EO)$_5$ in the other molecule is around 3.0 Å, typical of very weak hydrogen bonding. The T$_6$ segments are far from each other, adsorbed parallel to the graphite planes, at an equilibrium distance of 3.5−3.6 Å from the graphite sheet. The interaction between the molecules is weak ($E_{b,M-M}$ of around −20 kJ/mol) compared to the interaction between one molecule and the substrate (ΔE_{ads} = −589.1 kJ/mol). We could not identify a denser packing that would allow for commensurability of the substituents with the substrate.

AFM studies have revealed that, on top of this monolayer, layered islands form (Figure 2b, islands appearing in bright), with approximately the same thickness as those formed on mica. The monolayer is therefore acting as a new substrate, on top of which the molecules assemble probably with their long axes almost perpendicular to the plane of the underlying layer.

For (EO)$_5$−T$_6$−(EO)$_5$, the AFM and STM data show fibrillar structures in which the molecules are parallel to each other, with their T$_6$ segment probably in an edge-on or tilted orientation with respect to the graphite plane. Simulations of stacks of a few molecules have therefore been carried out starting from the π-stack conformation reminiscent of that of T$_6$. A cluster of eight molecules has been built in a a × 13; b × 30 graphite periodic cell, starting from a distance of 4 Å between the molecules and the graphite sheet. The width of the periodic cell is chosen to allow sizable interactions between molecules in adjacent stacks, since it has been shown that fibrillar structures are made of one-molecule-wide rows, parallel to each other. The results of the MD simulation at 300 K are illustated in Figure 6c. All extracted stable structures show an orientation

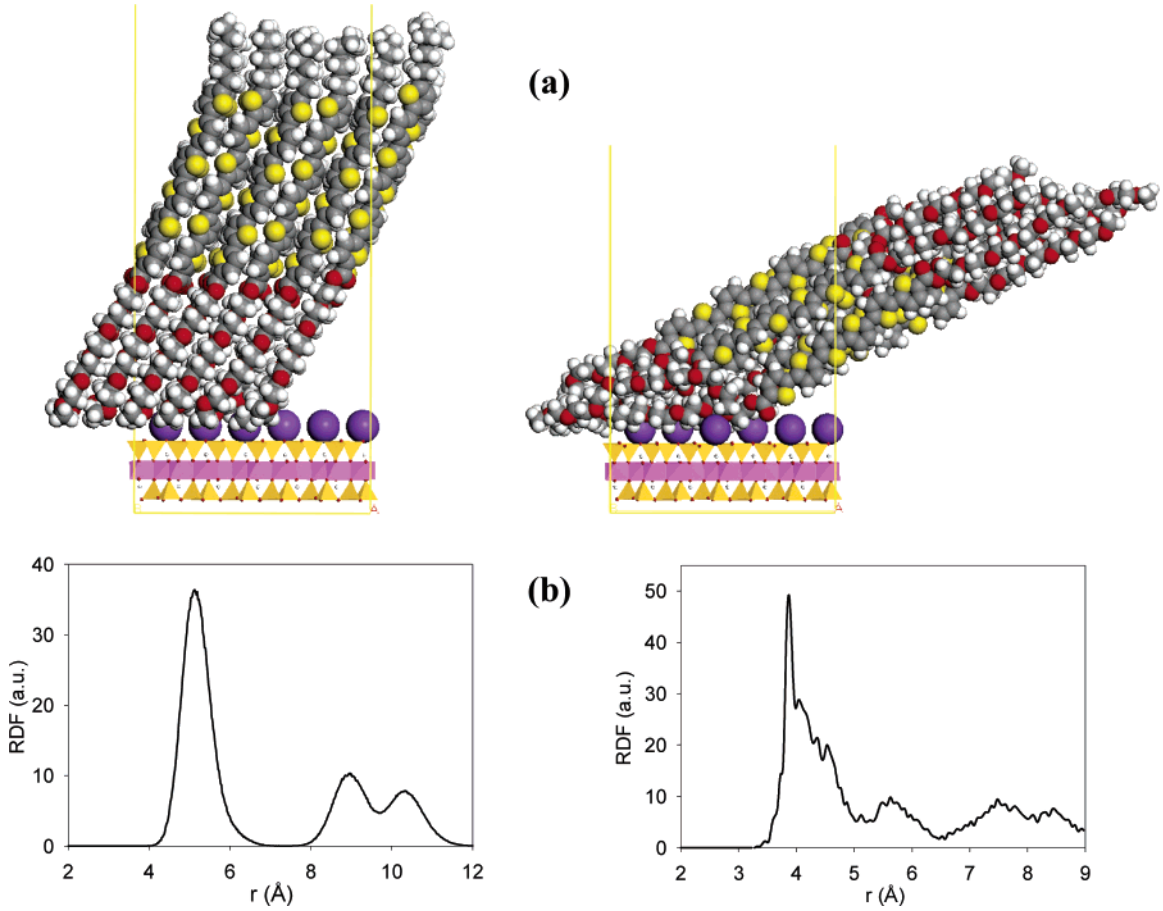

Figure 7. Molecular modeling of $(EO)_5-T_6-Hex$ (left) and $(EO)_5-T_6-(EO)_5$ (right) on muscovite mica (4 × 3 cell, with periodic boundaries in yellow). (a) Stable structure. (b) Radial distribution function over the whole MD simulation between equivalent carbon atoms of the T_6 segments.

of the conjugated planes perpendicular, edge-on to the substrate plane, with an equilibrium distance of 2.7 Å between graphite and the nearest atoms (hydrogen atoms) of the molecules. The T_6 segments remain parallel to each other during the whole simulation, at a constant distance of 3.7 Å. The regularity of the T_6 packing is reflected by the RDF between carbon atoms of adjacent molecules, Figure 6d, which shows sharp peaks (i.e., small deviation) around the integer multiples of this distance. The $(EO)_5$ segments remain more or less extended along the direction of the T_6 segment, and a few of them move out of the stacking plane, due to steric hindrance; see Figure 6c, bottom.

3.4.2. Structural Order in Stacks on Mica. For $(EO)_5-T_6-$Hex on mica, the AFM data suggest that, within the monolayers, the molecules are almost fully extended, perpendicular to the substrate plane. This type of structure is reminiscent of those of T_6 or $Hex-T_6-Hex$ on polar substrates;[22] in this case, the molecules weakly interact with the substrate and arrange in herringbone-type layered crystals. Therefore, we started from this type of arrangement with all side groups of one type ($(EO)_5$ or hexyl) on the same side of the T_6 stack, because (i) the $(EO)_5-(EO)_5$ and alkyl−alkyl interactions are more favorable than (EO)−alkyl mixed interactions and (ii) the different segments have different lengths and mixing them would be detrimental for T_6 stacking, which globally drives the assembly. We have built a cluster of 24 fully extended molecules in a $a \times 4$; $b \times 3$ periodic cell; note that we have started with the $(EO)_5$ segments in interaction with the mica, since it is the most likely configuration; see section 3.2. Upon a 300 ps MD simulation at 300 K, the herringbone arrangement is found to be very stable. The corresponding structure is shown in Figure 7a (left), with the fully extended molecules almost perpendicular to the substrate plane. (The T_6 axis is tilted by about 20° with respect to the normal to the substrate.) The distance between the basal mica plane and the terminal atom of the top of the stack (hydrogen of the hexyl segment) stabilizes around 46 Å, in full agreement with the AFM-measured thickness of the layers (4.7 ± 0.2 nm). In terms of structural order, the herringbone arrangement prevails during the whole MD, and the RDF of equivalent carbon atoms of the T_6 segments shows the typical shape corresponding to the interchain distances of the crystalline herringbone motif (nearest distance between equivalent carbon atoms of 5.0 Å); see Figure 7b, left.

AFM experiments on $(EO)_5-T_6-(EO)_5$ thin deposits on mica have shown monolayers with a constant thickness of 2.7 ± 0.2 nm. In this case, the molecules are not fully extended perpendicular to the substrate plane, since the length of the molecule is 6.5 nm. They are not fully extended parallel to the substrate plane either since in this case the thickness would be only a few angstroms. Several initial stacking geometries of 12 molecules on a mica $a \times 4$; $b \times 3$ periodic cell (that correspond to the same density as in the previous case) were considered. In all cases, the molecules were randomly placed at a distance of a few angstroms to each other. After having carried out a preliminary MM simulation, we apply a MD run at 300 K. During the simulation, the angle between the T_6 long axes and mica plane evolves until it stabilizes around 30−35°. The most probable stacking structure is shown in Figure 7a, right; the $(EO)_5$ groups at the bottom of the stack are coiled to maximize the interaction with the K^+ ions (mauve), while the $(EO)_5$ groups at the top of the stack are almost fully extended along the T_6 long axis. The distance between a terminal hydrogen atom on top of the stack and the basal mica plane evolves more or less

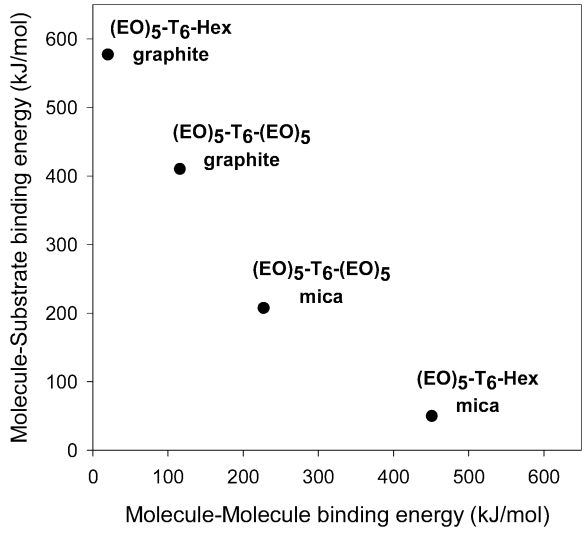

Figure 8. Molecule−substrate vs molecule−molecule binding energies (in absolute value) for the different systems.

strongly during the MD (depending on the initial configuration) and eventually becomes almost constant around 26 Å, in agreement with the experimental value of the thickness of the layers (2.7 ± 0.2 nm). In terms of the interchain distance, the RDF between equivalent carbon atoms of T_6 segments (Figure 7b, right) shows a peak at 3.9 Å, meaning that the molecules are close-packed, even though the molecular arrangement is less regular than in the herringbone structures of $(EO)_5-T_6-Hex$, as suggested by the shape of the curve above 3.9 Å. Such a value for the interchain distance indicates that the T_6 segments are π-stacked locally.

4. Comparison between Molecule−Molecule and Molecule−Substrate Interactions

Globally, the modeled structures are in very good agreement with the observed morphologies, and all situations correspond to a balance between molecule−molecule and molecule−substrate interactions, with different relative weights from case to case. To provide an insight into this issue, we define two types of *binding energy per molecule*: (i) for molecule−molecule interactions, $E_{b,M-M}$ as defined in section 3.3 ($E_{b,M-M} = (E_{stack} - nE_{molec})/n$); (ii) for molecule−substrate interactions, $E_{b,M-S} = (E_{tot} - E_{subst} - E_{stack})/n$, E_{stack} being the energy of the stack alone in the same configuration as in the total system, E_{subst} the energy of the substrate alone, and n the number of molecules in the stack. All of the energy values are calculated under periodic boundary conditions (except obviously E_{molec}). In Figure 8, we plot the absolute values of $E_{b,M-S}$ versus the absolute values of $E_{b,M-M}$. This graph is an "energy map" showing this balance for the different systems (different molecules/stacking configurations on different substrates). It clearly appears that, on graphite, the molecule−substrate interactions are very large compared to molecule−molecule interactions. This leads to the structures where the molecules orient with their long axis parallel to the substrate, either "flat" ($(EO)_5-T_6-Hex$) or "edge-on" ($(EO)_5-T_6-(EO)_5$). Although the molecules are quite similar in structure, this difference can be rationalized by the fact that, as described in section 3.3, polar groups (in this case $(EO)_5$) in both α- and ω-positions of the conjugated oligomer promote π-stacking, at least if sufficient interactions with the substrate are present, which is the case with graphite (edge-on orientation leads to sizable T-shape interactions with graphite). For stacks of $(EO)_5-T_6-(EO)_5$ on mica, the two binding energies are almost identical, meaning that in this case a balance exists between intermolecular interactions and interactions with the substrate. For stacks of $(EO)_5-T_6-Hex$ on mica (as in T_6 on mica), the intermolecular interactions are very large in the herringbone structure, while the fact that the molecules are with their long axis almost perpendicular to the substrate reflects very weak molecule−substrate interactions.

Let us now connect the data of Figure 8 with the experimental microscopic morphologies shown in section 3.1.

(1) When the strength of molecule−molecule and molecule−substrate interactions is similar ($(EO)_5-T_6-(EO)_5$ on mica), we observe 2D, layer-by-layer growth.

(2) When the molecule−molecule interactions are very strong compared to molecule−substrate interactions ($(EO)_5-T_6-Hex$ on mica), three-dimensional growth into layered islands is observed.[35]

(3) For deposits on graphite, the molecule−substrate interactions are larger than the molecule−molecule interactions for both molecules; this rationalizes the fact that the molecular orientation within the "flat" monolayer (in the case of $(EO)_5-T_6-Hex$) and the orientation of the 1D fibrils (in the case of $(EO)_5-T_6-(EO)_5$) correspond to (pseudo)epitaxial growth of these self-assembled structures.

5. Conclusion

These studies of the self-assembly at surfaces of oligothiophenes end-capped with oligo(ethylene oxide) or hexyl groups have shown that the molecule−molecule (or intersegment) interactions and the molecule−substrate interactions are both at work and lead to well-defined nanostructures, from 2D ultrathin regular layers (on mica) to 1D fibrillar objects (on graphite). The joint experimental studies of the morphology at the nanometer scale (via STM/AFM) and molecular modeling (via the atomistic MM/MD approach) appear most helpful to understand the impact of these interactions on the self-assembly of these conjugated molecules, which is of utmost importance in the performances of organic semiconductor devices such as OFETs. Note that those end-capped molecules have recently been used in OFET devices;[36] the active layer has a layered morphology (on SiO_2 dielectric), with approximately the same layer thickness as that observed here on mica. The devices show promising performances, with a current on/off ratio of 10^3 to 10^5 and with a charge mobility up to 2×10^{-2} $cm^2/(V\ s)$ (in the hole transport regime), which is among the best values for devices prepared from solutions. Moreover, the molecules containing hexyl groups (as $(EO)_5-T_6-Hex$) showed higher mobility than those bearing two (EO) groups (as $(EO)_5-T_6-(EO)_5$), consistent with the highly ordered structures they form and larger intermolecular $\pi-\pi$ interactions in the case of $(EO)_5-T_6-Hex$ on polar substrates. In terms of perspectives, the present results could be exploited for the construction of OFETs with selected well-defined structures. For instance, one will be able to compare the charge transport in 1D or 2D structures using the same material by tuning the nature of the (dielectric) substrate.

Acknowledgment. The collaboration between Mons and Leuven is conducted in the framework of the InterUniversity Attraction Pole Program (PAI V/3) of the Belgian Science Policy Office. The collaboration between Mons and Durham has been conducted within the European Commission Training and Mobility of Researchers Network LAMINATE (Large Area Molecular Electronics Involving a Novel Approach to Training

and Education—Contract No. HPRN-CT-2000-00135). Research in Mons is partly supported by the Government of the Region of Wallonia (Phasing Out Hainaut) and the Belgian National Fund for Scientific Research FNRS/FRFC. Ph.L. is a research Associate of the FNRS (Belgium). S.D.F. is a postdoctoral fellow of the Fund for Scientific Research, Flanders.

TABLE 1A: Atomic Charges of the Muscovite Mica

atom	description	charge
K	potassium ion at the surface	+1.00
Si	silicon in tetrahedral layer	+1.20
Al	aluminum in octahedral layer	+3.00
O	oxygen in tetrahedral layer (bridge)	−0.99
O(H)	hydroxyl oxygen in octahedral layer	−1.42
H	hydroxyl hydrogen in octahedral layer	+0.72

References and Notes

(1) Salaneck, W. R.; Stafström, S.; Brédas, J. L. *Conjugated Polymers Surfaces and Interfaces*; Cambridge University Press: New York, 1996.

(2) (a) Horowitz, G. *Adv. Mater.* **1998**, *10*, 365. (b) Cornil, J.; Beljonne, D.; Calbert, J.-P.; Brédas, J. L. *Adv. Mater.* **2001**, *13*, 1053. (c) Dimitrakopoulos, C. D.; Malenfant, P. R. L. *Adv. Mater.* **2002**, *14*, 99.

(3) Halik, M.; Klauk, H.; Zschieschang, U.; Schmid, G.; Ponomarenko, S.; Kirchmeyer, S.; Weber, W. *Adv. Mater.* **2003**, *15*, 917.

(4) Dinelli, F.; Murgia, M.; Levy, P.; Cavallini, M.; Biscarini, F.; De Leeuw, D. M. *Phys. Rev. Lett.* **2004**, *92*, 116802.

(5) For example, see: (a) Fichou, D. *Handbook of Oligo- and Polythiophenes*; Wiley-VCH: New York, 1999. (b) Garnier, F.; Hajlaoui, R.; Yassar, A.; Srivastava, P. *Science* **1994**, *265*, 1684. (c) Sirringhaus, H.; Brown, P. J.; Friend, R. H.; Nielsen, M. N.; Bechgaard, K.; Langeveld-Voss, B. M. W.; Spiering, A. J. H.; Janssen, R. A. J.; Meijer, E. W.; Herwig, P.; de Leeuw, D. M. *Nature* **1999**, *401*, 685.

(6) Leclère, Ph.; Surin, M.; Viville, P.; Lazzaroni, R.; Kilbinger, A. F. M.; Henze, O.; Feast, W. J.; Cavallini, M.; Biscarini, F.; Schenning, A. P. H. J.; Meijer, E. W. *Chem. Mater.* **2004**, *16*, 4452.

(7) For oligothiophene assembly on different substrates, see: (a) Lang, P.; Ardhaoui, M. E.; Wittmann, J. C.; Dallas, J. P.; Horowitz, G.; Lotz, B.; Garnier, F.; Strupe, C. *Synth. Met.* **1997**, *84*, 605. (b) Prato, S.; Floreano, L.; Cvetko, D.; De Renzi, V.; Morgante, A.; Modesti, S.; Biscarini, F.; Zamboni, R.; Taliani, C. *J. Phys. Chem. B* **1999**, *103*, 7788. (c) Azumi, R.; Götz, G.; Debaerdemaeker, T.; Bäuerle; P. *Chem.—Eur. J.* **2000**, *6*, 735. (d) Böhme, O., Ziegler, Ch.; Göpel, W. *Synth. Met.* **1994**, *67*, 87. (d) Chang, P. C.; Lee, J.; Huang, D., Subramanian, V.; Murphy, A. R.; Fréchet, J. M. J. *Chem. Mater.* **2004**, *16*, 4783.

(8) For a review on the structural order in pentacene layers, see: Ruiz, R.; Choudhary, D.; Nickel, B.; Toccoli, T.; Chang, K.-C.; Mayer, A. C.; Clancy, P.; Blakely, J. M.; Headrick, R. L.; Iannotta, S.; Malliaras, G. M. *Chem. Mater.* **2004**, *16*, 4497.

(9) Fichou, D. *J. Mater. Chem.* **2000**, *10*, 571.

(10) (a) Horowitz, G.; Peng, X.-Z.; Fichou, D.; Garnier, F. *Synth. Met.* **1992**, *51*, 419. (b) Wang, G.; Moses, D.; Heeger, A. J.; Zhang, H.-M.; Narasimhan, M.; Demaray, R. E. *J. Appl. Phys.* **2004**, *95*, 316.

(11) Zangh, Y.; Lu, R.; Liu, Q.; Song, Y.; Jiang, L.; Liu, Y.; Zhao, Y.; Li, T. J. *Thin Solid Films* **2003**, *437*, 150.

(12) Henze, O.; Parker, D.; Feast, W. J. *J. Mater. Chem.* **2003**, *13*, 1269.

(13) (a) Rappé, A. K.; Casewit, C. J.; Colwell, K. S.; Goddard, W. A., III.; Skiff, W. M. *J. Am. Chem. Soc.* **1992**, *114*, 10024. (b) Casewit, C. J.; Colwell, K. S.; Rappé, A. K. *J. Am. Chem. Soc.* **1992**, *114*, 10035 (c) Casewit, C. J.; Colwell, K. S.; Rappé, A. K. *J. Am. Chem. Soc.* **1992**, *114*, 10046.

(14) Gaudel-Siri, A.; Brocorens, P.; Siri, D.; Gardebien, F.; Brédas, J. L.; Lazzaroni, R. *Langmuir* **2003**, *19*, 8287.

(15) Brigatti, M. C.; Frigieri, P.; Poppi, L. *Am. Mineral.* **1998**, *83*, 775.

(16) Greathouse, J. A.; Refson, K.; Sposito, G. *J. Am. Chem. Soc.* **2000**, *122*, 11459.

(17) (a) Müller, K.; Chang C. C. *Surf. Sci.* **1969**, *14*, 39. (b) Campbell, P. A.; Sinnamon, L. J.; Thompson C. E.; Walmsley D. G. *Surf. Sci.* **1998**, *410*, 768.

(18) Odelius, M.; Bernasconi, M.; Parinello, M. *Phys. Rev. Lett.* **1997**, *78*, 2855.

(19) The crystallographic parameters of graphite are from: McKie, D.; McKie, C. *Essentials of Crystallography*; Blackwell Scientific Publications: Boston, 1986.

(20) Biscarini, F.; Zamboni, R.; Samori, P.; Ostoja, P.; Taliani, C. *Phys. Rev. B* **1995**, *52*, 14868.

(21) Hotta, S.; Waragai, K. *Adv. Mater.* **1993**, *5*, 896.

(22) Garnier, F.; Yassar, A.; Hajlaoui, R.; Horowitz, G.; Deloffre, F.; Servet, B.; Ries, S.; Alnot, P. *J. Am. Chem. Soc.* **1993**, *115*, 8716.

(23) Barabási A.-L. and Stanley, H. E. *Fractal Concepts in Surface Growth*; Cambridge University Press: Cambridge, U. K., 1995.

(24) Schenning, A. P. H. J.; Kilbinger, A. F. M.; Biscarini, F.; Cavallini, M.; Cooper, H. J.; Derrick, P. J.; Feast, W. J.; Lazzaroni, R.; Leclère, Ph.; McDonell, L. A.; Meijer, E. W.; Meskers, S. C. J. *J. Am. Chem. Soc.* **2002**, *124*, 1269.

(25) De Feyter, S.; De Schryver, F. C. *Chem. Soc. Rev.* **2003**, *32*, 139.

(26) Lazzaroni, R.; Calderone, A.; Brédas, J. L.; Rabe, J. P. *J. Chem. Phys.* **1997**, *107*, 99.

(27) Stabel, A.; Rabe, J. P. *Synth. Met.* **1994**, *67*, 47.

(28) The RDF is the spherically averaged distribution of interatomic distances during the MD run.

(29) Rabe, G. W.; Heise, H.; Liable-Sands, L. M.; Guzei, I. A.; Rheingold, A. L. *J. Chem. Soc., Dalton Trans.* **2000**, 1863.

(30) Bunz, U. H. F. *Chem. Rev.* **2000**, *100*, 1605.

(31) (a) Buchholz, S.; Rabe, J. P. *Angew. Chem., Int. Ed. Engl.* **1992**, *31*, 189. (b) Arnold, T.; Thomas, R. K.; Castro, M. A.; Clarke, S. M.; Messe, L.; Inaba, A. *Phys. Chem. Chem. Phys.* **2002**, *4*, 345.

(32) (a) Paserba, K.; Gellman, A. J. *Phys. Rev. Lett.* **2001**, *86*, 4338. (b) Gellman, A. J.; Paserba, K. P. *J. Phys. Chem. B* **2002**, *106*, 13231.

(33) Curtis, M. D.; Cao, J.; Kampf, J. W. *J. Am. Chem. Soc.* **2004**, *126*, 4318.

(34) Horowitz, G.; Bachet, B.; Yassar, A.; Lang, P.; Demanze, F.; Fave, J.-L.; Garnier, F. *Chem. Mater.* **1995**, *7*, 1337.

(35) In the layered islands of $(EO)_5-T_6-Hex$ on mica, the estimated binding energy between a stack of 18 molecules in a layer and a single molecule in the layer on top, i.e., $E_{b,M-M}$ between layers, is around 20 kJ/mol.

(36) Sandberg, H. G. O.; Henze, O.; Sirringhaus, H.; Kilbinger, A.; Feast, W. J.; Friend, R. H. *Proc. SPIE—Int. Soc. Opt. Eng.* **2001**, *4466*, 35.